Transient Stability Improvement of a Hybrid Power System: A Novel Configuration of Compensating Type Custom Power Devices and Fault Current Limiters

Shahab Khormali[1*], Salman Amirkhan[2,3], Ramin Mokhtari[2,3], Hassan PourvaliSouraki[3,4], Tatiana Kováčiková[1], Masoud Radmehr[2,3], Azadeh Sadat Naeimi[3,5]

Abstract–Applying distributed energy resources (DERs) to power systems has been promoted as a promising option to meet the growing electricity demand. Despite significant economic, environmental, and resiliency benefits, integrating DER, including power electronic devices, into the existing power networks causes stability and power quality issues. Therefore, to meet stability and power quality standard limits, a sort of compensation using cost-effective and energy-efficient technologies and power electronics-based concepts is needed. This paper presents a novel configuration of compensating type custom power devices (CPDs) and fault current limiters (FCLs) for limiting balanced and unbalanced faults and improving the transient performance of distributed generation (DG) sources in a hybrid power system. Moreover, three power grid operational scenarios are addressed to reflect the impact of the type of fault and variable power generation capacity of DGs on transient stability. Four configurations are implemented using two FCLs (BFCL and SFCL) and two energy compensation devices (DVR and UPQC). The transient performance of involved DGs with and without applying proposed compensation methods is simulated. Simulation experiments were carried out using MATLAB/SIMULINK software. The simulation results indicate that UPQC- BFCL is the best solution in all scenarios that improve the transient stability of the proposed power system under both balanced and unbalanced faults.

Keywords: custom power devices, dynamic voltage restorer, fault current limiter, transient stability, unified power quality conditioner.

1. Introduction

Integration of renewable energy sources (RESs) into the power grid is an effective solution in order to reduce the environmental impacts of conventional energy sources and meet the future electricity needs. Among different RESs, wind and solar are promising solutions that can be integrated as DG units into the modern power grids[1].

Nomenclature

AF	active filter
BFCL	bridge fault current limiter
BR	braking resistor
CPD	custom power device
DER	distributed energy resources
DFIG	doubly-fed induction generator
DG	distributed generation
DVR	dynamic voltage restorer
Eq	equation
FCL	fault current limiter
FRT	fault ride through
GS	grid side
GSC	grid side converter
HCLID	hybrid fault current limiter and interrupting device
HFCL	hybrid FCL
IGBT	insulated-gate-bipolar-transistor
LVRT	low voltage ride-through
NRA	network reconfiguration algorithm
PCC	point of common coupling
PI	proportional-integrator controller
RES	renewable energy source
RSC	rotor side convertor
RSCFCL	ring-based saturated core fault current limiter
R-SFCL	resistive super conductive fault current limiter

1* Corresponding Author: Department of International Research Projects (ERAdiate+), University of Žilina, Žilina, Slovakia.

Email:shahab.khormali@uniza.sk

2 Department of Electrical Engineering, Aliabad Katoul Branch, Islamic Azad University, Aliabad Katoul, Iran

3 Energy Research Center, Aliabad Katoul Branch, Islamic Azad University, Aliabad Katoul, Iran

4 Mapna Operation and Maintenance Co.,Tehran, Iran

5 Department of Physics, Aliabad Katoul Branch, Islamic Azad University, Aliabad Katoul, Iran

SC	short circuit
SCFCL	saturated core fault current limiter
SFCL	super conductive fault current limiter
SG	synchronous generator
SMES	superconducting magnetic energy storage
SSB	solid-state breaker
SSCL	solid-state current limiter
SSFCL	solid-state fault current limiter
SSTS	solid-state transfer switch
STATCOM	static synchronous compensator
UPQC	unified power quality conditioner
VSC	voltage source converter
Cp	power coefficient
D	diode
PV	photovoltaic
Pw	extracted wind power
Pbase	base power
PDGS	distributed generation source power
Rm	maximum resistance
Rsh	shunt resistance
Tsc	transition time
Vw	wind velocity
ρ	air density
λ	tip speed ratio
β	blade pitch angle
$V_{Grid\ side}$	grid side voltage
V_{ref}	reference voltage
V_{DVR_ref}	DVR reference voltage
V_{DVR}	DVR actual voltage
$V_{DG\ side}$	DGs side bus voltage
ΔP_{DFIG}	power deviation of the DFIG
$\Delta \omega_{DFIG}$	speed deviation of the DFIG
ΔV_{DFIGdc}	DC link voltage deviation of DFIG
$\Delta \delta_{SG}$	load angle deviation of SG
$\Delta \omega_{SG}$	rotor speed deviation of SG
ΔP_{SG}	power deviation of SG
1lg	single line-to-ground fault
3lg	three line-to-ground fault
dq	d and q-axis
ms	millisecond
pow	power
p.u.	per unit
spd	speed
vlt	voltage

However, despite the proven benefits of using RESs, large scale integration of wind and solar power into the existing and conventional SG-based power system increases the complexity of the power systems and causes some issues related to the system transient stability such as fault current, voltage and frequency fluctuations, and harmonics [2]–[5]. Significant of transient stability analysis and application of FCLs dealing with optimal control of the modern electrical power systems with multiple RES has been discussed in[6]. [4]–[7]review the fault current contribution of renewable distributed generation and critical challenges regarding integrating renewable DGs into the distribution system, focusing on short circuit current capability. In this context, [8], [9]explain the important details about short circuit (SC) faults as the most destructive faults in power systems generating fault current more than 20 times the maximum nominal current. [10]highlights several technical and economic-oriented drawbacks of the SC faults that negatively affect power systems. For example, DGs can lead to various problems in distribution systems. These problems include instances of unintended tripping caused by the operation of protection relays, compromised protection measures, and the inadvertent creation of isolated sections within the system during a short-circuit fault. The literature review reveals many proposed measures to overcome issues originating from SC faults ranging from traditional approaches to more advance approaches. Main features, advantages and disadvantages of both traditional and recently emerging FCL technologies have been discussed in[11]–[14]. [11]introduces technical features and major weaknesses of some of traditional approaches in the context of distribution systems which are applied for limiting the fault current levels. It underlines the grid complexity, power loss and reliability issues as the main difficulties of these methods. An assistance system for network operators dealing with fault levels exceeding the capacity of protective equipment was introduced in[12]. This system incorporates a network reconfiguration algorithm (NRA). The algorithm was implemented and tested on a medium-sized network to evaluate its effectiveness, yielding positive results. In[13], the focus is on examining how fault level constraints affect the economic operation of modern power systems. Compared to traditional approaches, FCLs technologies have drawn significant attention in recent years. In[14], a detailed examination of FCL technologies was conducted, explicitly highlighting their developmental and technical aspects. The authors classified FCLs into four primary categories: superconducting FCLs (SFCLs), solid-state FCLs (SSFCLs), hybrid FCLs (HFCLs), and various other technological variations. In[15], a study demonstrates the utilization of a customized flux-coupling SFCL configuration within an AC microgrid. This implementation

proves highly effective in constraining fault currents, ensuring power equilibrium, and improving voltage and frequency stability in the microgrid. Furthermore, the study in [16]explores the use of a resistive SFCL (R-SFCL) as a means to reduce fault currents in a self-sufficient microgrid operating with a dynamic load model and DGs.The utilization and development R-SFCLs were proposed by researchers in [17] as a means to effectively safeguard a DC microgrid against short circuit faults. The investigation carried out in [18]focused on the integration of SFCLs with batteries within an independent DC microgrid, yielding positive outcomes in terms of battery longevity, adherence to grid codes, and the cost of DC circuit breakers. Extensive analysis on the effects of SSFCLs on power system reliability and quality has been conducted in[19]–[22].In general, there are two main categories for FCLs and SSFCLs: resistive SSFCLs (referred to as R-type SSFCLs) and inductive SSFCLs (known as L-type SSFCLs). A recent study [23]introduces a novel SSFCL, termed LR-type SSFCL, which combines the advantages of both L-type SSFCLs and R-type SSFCLs. This innovation enhances the stability and overall quality of the power system. Current research has extensively explored the applications of hybrid FCLs in both AC and DC power networks. In [24], the authors analyze the performance of a hybrid fault current limiter and interrupting device (HCLID) technique in industrial applications at low and medium voltage levels, both in AC and DC systems. [25]describes a successful implementation of a hybrid SFCC (superconducting fault current controller) that operates independently of grid monitoring technology. It ensures proper coordination of protective devices and safe operation of a distributed generation (DG) microgrid. The effectiveness of the real-time application of saturated core FCL (SCFCL) and ring-based saturated core FCL (RSCFCL) in enhancing the fault ride-through (FRT) capability of a DFIG (doubly fed induction generator) system is demonstrated in [26]. The feasibility of ideal SCFCL and RSCFCL is validated through tests measuring their characteristics, including thermal radiation, under normal and fault conditions.

Apart from FCL technologies, power electronics-based technologies known as custom power devices (CPDs) have been developed to meet power quality problems in the electrical distribution system. About this matter, a study by [27]explores the notion of custom power. It classifies CPDs into two categories: network-reconfiguring type, which includes solid-state devices like current limiters (SSCL), breakers (SSB), and transfer switches (SSTS); and compensating type, which comprises distribution static compensators (DSTATCOM), dynamic voltage restorers (DVR), and unified power quality compensators (UPQC).Comprehensive review on different types of power quality issues, their characteristics and also basic concepts, design parameters and implementation of compensating type of CPDs in electrical machines have been provided in[28]. Performance analysis of DVR, UPQC and DSTATCOM considering various factors such as power rating, cost, speed of operation and harmonic reduction have been carried out in [29].

From the available literature, it becomes apparent that considerable worldwide efforts have been made to analyze technical and economic features of available FCL technologies as well as CPDs used in power utilities. Unlike previous research that only utilized either FCLs or CPDs, this study proposes a combined approach that includes both energy storing and losing characteristics simultaneously through configuring conventional FCLs (BFCL and SFCL) with energy compensating devices (DVR and UPQC). In this approach, the priority is to control the fault current through applying energy compensating and energy losing options, respectively. If it is not possible to handle occurred faults by energy compensating options, then system will use energy losing options.

In this study, a hybrid power system consists of SG, DFIG based wind turbine and PV array connected to an infinite bus has been modeled and impact of novel configurations of CPDs and FCLs on transient stability of the proposed hybrid system has been investigated. The paper contributes to:

- Analyzing technical features of conventional FCLs and CPDs applicable in a hybrid power system,
- Developing and analyzing DVR-BFCL, DVR-SFCL, UPQC-BFCL and UPQC-SFCL configurations,
- Simulating the transient responses of involved DG sources to the proposed energy compensators,
- Evaluating simulation results based on transient performance indices and selecting the best configuration enhancing power quality in the system under study.

The rest of the paper is organized as follows: the next section reviews modeling of the proposed hybrid microgrid, section 3 presents recommended FCLs, CPDs and configurations including control strategies. Power grid operation scenarios and simulation results, and conclusions are provided in section 4 and section 5, respectively.

2. Modeling of power grid under study

The model of the hybrid microgrid understudy will be presented in this section. Fig. 1 illustrates the structure of the microgrid consists of a SG (100 KVA), a DFIG wind turbine (150 KVA), and a PV array (100 kW) that are connected to an infinite bus through a double-circuit transmission line. Characteristics of DGs are provided in Tables 7 and 8 in the appendix. The DVR, UPQC, BFCL and SFCL are connected between the PCC bus and the infinite bus (in series at the terminal of the PCC). Characteristics of FCLs and CPDs are also available in the appendix, Tables 9, 10, 11, and 12. The power base and frequency base rates of the system are 100 KVA and 60 Hz, respectively.

Fig. 1. General structure of hybrid microgrid under study.

2.1 Modeling of wind turbine

Fig. 2 [30]showcases the schematic diagram depicting the structure of DFIG. DFIG encompasses two converters, namely the grid-side converter (GSC) and the rotor-side converter (RSC), which are independently controlled. The central concept involves the RSC's regulation of active and reactive power by manipulating rotor current components. At the same time, the GSC manages the DC link voltages and maintains converter functionality at a power factor of unity (eliminating reactive power)[31].To ensure effective control of RSC, it is necessary to obtain the rotor current measurements in the dq-frame, namely I_{dwr_mes} and I_{qwr_mes}. These measurements are used to follow the reference currents generated by the real power and the magnitude of the stator voltage setting. For reference, please refer to Fig. 3(a), which illustrates the block diagram of the RSC control system. Similarly, the stator current measurements in the dq-frame, namely I_{ds_mes} and I_{qs_mes}, should accurately track the reference current in the dq-frame (I_{d_ref} and I_{q_ref}). This tracking is crucial for maintaining a constant DC link voltage and achieving a unity power factor at the output of the GSC converter. To better understand this control system, you can refer to Fig. 3(b), which depicts the block diagram of the GSC control system[32].

Fig. 2. Doubly-fed induction generator system diagram [30].

The mechanical power extraction from wind can be expressed as follows[32].

$$P_w = 0.5 * \rho * \pi * R^2 * V_w^3 * C_p(\lambda, \beta) \qquad (1)$$

where P_w and V_w are power extracted from the wind and wind velocity, respectively. ρ represents the air density, and C_p indicates the power coefficient, which is the function of tip speed ratio (λ) and blade pitch angle (β). R represents the blade radius in meters.

Fig. 3. Control systems considered for (a) DFIG RSC, (b) DFIG GSC [32].

2.2 Modeling of PV system

The PV plant comprises a combination of PV modules connected in a series-parallel configuration to achieve the desired power output. It is linked to the Point of Common Coupling (PCC) through a boost converter and an aggregated DC to AC inverter. Fig. 4 illustrates the layout of grid-connected converters and PV systems. For this research, a PV plant with a capacity of 100 kW is constructed by connecting 100 PV modules in series and 50 branches in parallel. The KC200GT PV module [6] is employed in this study, providing a peak power of 200 W. The Perturb and Observe (P&O) MPPT [6]technique is applied to the boost converter to ensure optimal power extraction from the PV module under various environmental conditions. In order to interface with the grid, a three-level, three-phase voltage source converter (VSC) is utilized to convert the DC power into AC power. Fig. 5 illustrates the block diagram depicting the control of the VSC.
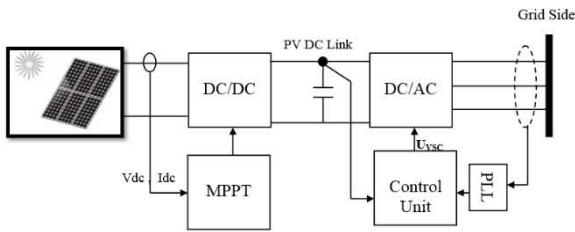
Fig. 4. Structure of PV system including converters.
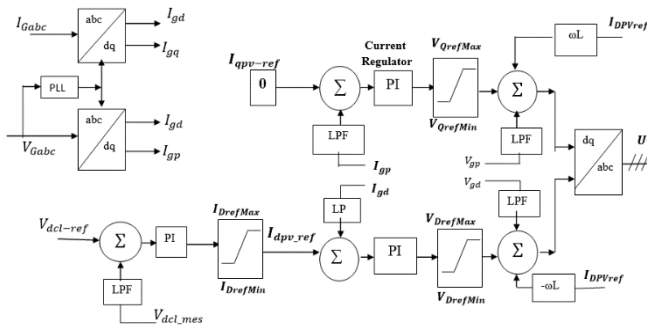
Fig. 5. Control system designed for PV inverter.

2.3 Modeling of synchronous generator

In this study, we used the equations presented in reference [33] to characterize the SG. Our model incorporates a rotor dq-axis as a point of reference, rotating at the speed of the rotor. The relevant SG parameters can be found in the appendix to ensure accurate design considerations.

3. Structures and control mechanisms of the proposed FCLs and CPDs

3.1 Bridge fault current limiter (BFCL)

Fig. 6 shows the structure of the bridge fault current limiter (BFCL) [28]–[31]used in this study, including two branches: the bridge part and the shunt branch. In normal operation, the closed IGBT switch allows the positive half of the line current to flow through diodes D1, D4, and the bridge components. Conversely, during the negative half cycle of the line current, it passes through D3, L_{dc}, S, and D2. In the event of a fault on the transmission line, the controller opens the IGBT switch, redirecting the line current to follow the path of the shunt branch.
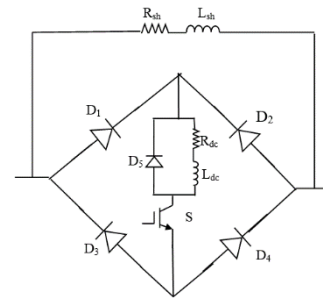
Fig. 6. Structure of bridge fault current limiter.

The design considerations incorporate specific equations (2) and (3) to determine the BFCL parameters[31].

$$P_{BFCL} \leq \frac{P_{DGS}}{3} \tag{2}$$

$$P_{BFCL} = I_{SC}{}^2 R_{sh} \tag{3}$$

where $P_{DGS} = P_{SG} + P_{PV} + P_{DFIG}$ is 350 *kW*, base power P_{base}= 100 *KVA* and R_{sh} = *0.286 p.u.*

3.2 Superconducting fault current limiter (SFCL)

In relation to power system stability, SFCL is acknowledged as an effective technology that enhances stability. SFCL is recognized as a self-repairing technology since it eliminates the need for control actions or human involvement. It achieves this by automatically detecting excessive current and recovering from a non-superconducting state to a superconducting one. By utilizing SFCL, the fault current is efficiently suppressed, reducing the voltage dip at the terminals of wind power plants. Consequently, this expands the voltage safety margin of the low-voltage ride-through (LVRT) curve [34].

In general, high-temperature SFCLs can be classified into resistive, inductive, and hybrid types. However, for the purpose of this study, a resistive SFCL was utilized. The SFCL can be characterized by impedance, which is influenced by current and temperature, or by resistance,

which changes over time. The latter representation is more direct and enables a reduction in simulation time. In the event of a fault, the time needed to restore stability in an electric power grid is several seconds. Consequently, it is unnecessary to employ an accurate SFCL model for our specific case. For the simulation, the SFCL employed can be depicted by a time-varying resistance according to the following [33]:

$$R_{SFCL} = R_m(1 - exp(-t/T_{sc})) \qquad (4)$$

where R_m represents the maximum resistance that SFCL can provide, and Tsc denotes the transition time from the superconducting state to the normal state. R_m and Tsc have been assumed 0.4 ohms and 1 ms, respectively [33].

Fig. 7 represents the developed SFCL model including fault sensing block, which calculates the difference between measured current and predetermined critical current. Parameters of the proposed SFCL technology have been provided in the appendix.
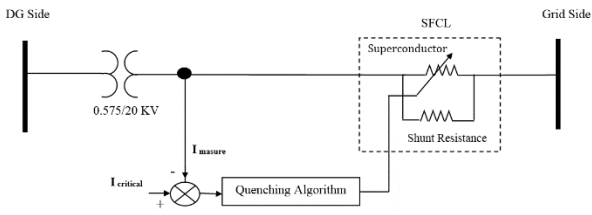
Fig. 7. Structure of superconducting fault current limiter.

3.3 Dynamic voltage restorer (DVR)

DVR is a widely recognized device connected in series to ensure a consistent root mean square (rms) voltage at the wind generator terminal, even during events like voltage sags and faults. To maintain a constant and synchronized voltage at the point of common coupling (PCC) with the main network, the DVR was utilized in this experiment to introduce an optimal voltage injection into the grid bus.Fig. 8 depicts the structure of DVR utilized in this study. To provide the compensating voltage, DVR is equipped with a capacitor increasing the ride-through capability of DVR. Capacitor size is characterized as a time constant (T) calculated based on the ratio of the rated DC voltage link (V_{DClink}) and the rated apparent power (S_{DVR}) of the converter, as shown in Eq 5 [35]. DVR parameters are presented in the appendix.

$$T = \frac{1}{2} \frac{CV_{DClink}^2}{S_{DVR}} \qquad (5)$$
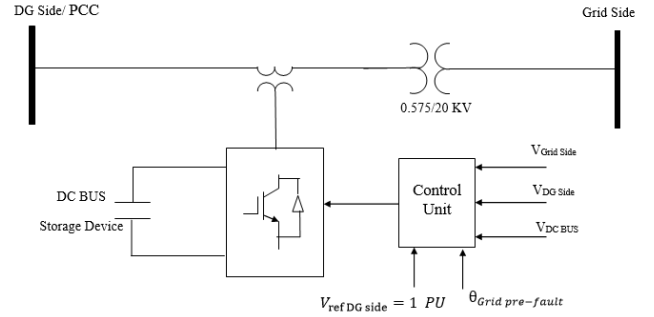
Fig. 8. Structure of dynamic voltage restorer.

3.4 Control mechanism of dynamic voltage regulator (DVR)

This section elucidates the control mechanism responsible for governing the operational aspects of a DVR in both regular and faulty scenarios. The calculation of the disparity between the voltage on the grid side ($V_{Grid side}$) and the reference voltage (V_{ref}) yields the DVR reference voltage (V_{DVR_ref}). Additionally, the actual voltage of the DVR (V_{DVR}) is ascertained by computing the difference between the voltage on the DG side bus ($V_{DG side}$) and the reference voltage (V_{ref}) within the dq-frame.

The system employs a closed-loop control strategy that combines feedforward compensation and a fuzzy feedback regulator. This control scheme aims to mitigate the variance between the actual voltage of the DVR (V_{DVR}) and the desired reference voltage (V_{DVR_ref}), as depicted in Fig. 9 [36]. Consequently, the regulated voltage is converted into a three-phase reference voltage, which is then utilized to generate pulses for the IGBT inverter. Detailed parameters of the DVR device can be found in the appendix.
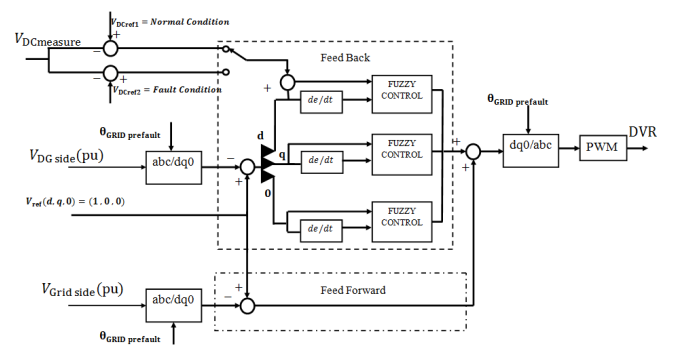
Fig. 9. Structure of the control system designed for DVR converter.

3.5 Unified power quality conditioner (UPQC)

UPQC is a specialized power device comprising two voltage source inverters (VSI) that are linked to a direct current (dc) energy storage capacitor. Fig. 10 illustrates the schematic diagram of the UPQC. The sizing of the UPQC capacitor is determined using the same Eq 5 as the DVR

capacitor. The parameters of the UPQC can be found in the appendix (Table 12).
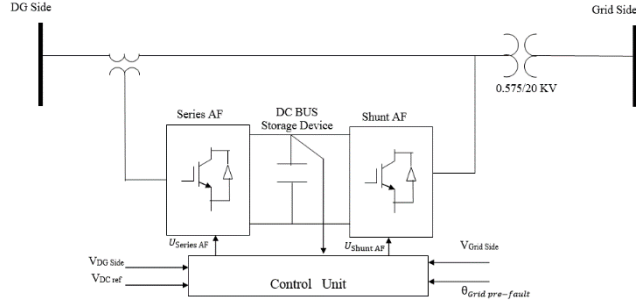
Fig. 10. Structure of unified power quality conditioner.

3.6 Control mechanism of unified power quality conditioner

As illustrated in Fig. 10, UPQC contains two active filters (AF): series AF and shunt AF. Each AF needs to be controlled to meet UPQC control requirement. Fig. 11 (a) depicts the series AF controller which is similar to DVR controller illustrated in the previous section, but DC link voltage is controlled with parallel active filter controller. Fig. 11 (b) shows shunt active filter control block diagram where amplitude and phase of injected current with shunt active filter is dependent on dc link voltage and line voltage phase, respectively.
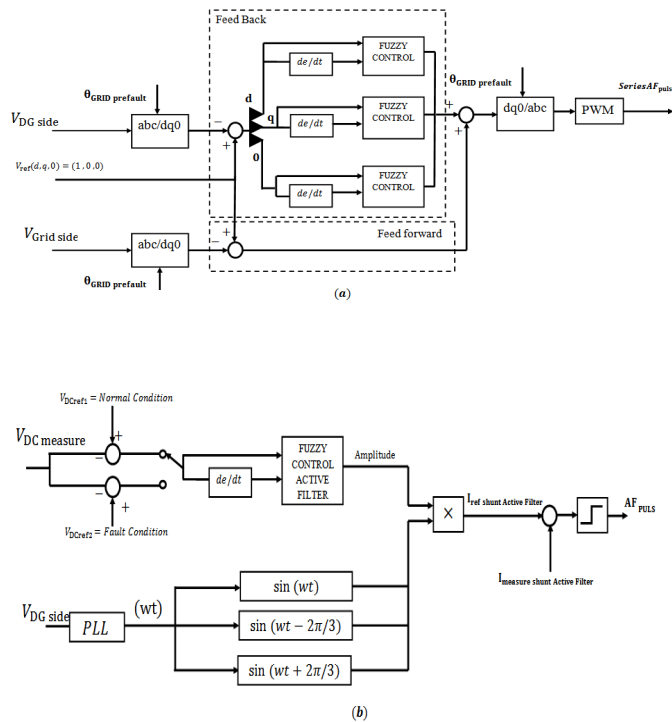
Fig. 11.(a) UPQC series AF controller (b) UPQC shunt AF controller.

3.7 Operating mechanism of FCL and CPD under normal and fault conditions

As mentioned earlier, this research work contributes to investigating the impact of novel configurations of CPD and FCL on the transient stability of power systems. In other words, the aim is to simultaneously benefit from both the energy compensating capacity of CPDs and the fault limiting character of FCL during fault conditions. Therefore, four different configurations (DVR-BFCL, DVR-SFCL, UPQC-BFCL, and UPQC-SFCL) have been considered. It should be highlighted that the main idea is to prioritize the utilization of the energy storing capacity of DVR and UPQC during the fault condition. Table 1 presents the operating mechanism of FCLs and CPDs under fault and normal conditions formulated as a four-step process. Step 1 represents the fault detection state (Fault=1) with available energy storing capacity (capacity=1) in DVR and UPQC. At this step, the control system prioritizes CPDs (DVR, UPQC) in each configuration to charge their limited storage devices (DVR/UPQC charge=1, discharge=0) and keeps FCLs out of the operation (BFCL/SFCL=0). Since DVR and UPQC have limited storage capacity, step 2 indicates an operational situation under the fault (Fault=1) with no more energy storing capacity (Capacity=0) in CPDs (DVR/UPQC charge=0, discharge=1). Under this condition, the control system brings into force the FCLs' well-known energy losing feature to limit the fault (BFCL/SFCL=1). Step 3 corresponds to a normal operating form (Fault=0, BFCL/SFCL=0) with fully charged CPDs (Capacity=0, DVR/UPQC charge=0, discharge=1) injecting the stored energy into the grid. Accordingly, the energy-storing capacity state is changed from 0 to 1, which is addressed in step 4. It is the last step in the proposed operating loop representing no-fault situation (Fault=0) and both FCLs and CPDs are out of operation (DVR/UPQC charge=0, discharge=0, BFCL/SFCL=0).

Table 1. Operating mechanism of FCLs and CPDs under fault and normal conditions.

Step	Fault	CPD storing capacity	DVR/UPQC		BFCL/SFCL
			Charge	Discharge	
1	1	1	1	0	0
2	1	0	0	0	1
3	0	0	0	1	0
4	0	1	0	0	0

3.8 Index-based transient stability performance

The impact of the FCL-CPD proposal on the transient stability of the power system under study has been analyzed employing the performance indices presented in Eq (6). Transient responses of the grid generating components to utilizing different fault limiting techniques (BFCL, SFCL,

DVR/BFCL, DVR/SFCL, UPQC/BFCL, and UPQC/SFCL) under fault and normal situations are examined.

$$DFIG_{Pow}(PU.\sec) = \int_0^T |\Delta P_{DFIG}| dt$$

$$DFIG_{Spd}(PU.\sec) = \int_0^T |\Delta \omega_{DFIG}| dt$$

$$DFIG_{Vter\min al}(PU.\sec) = \int_0^T |\Delta V_{DFIGdc}| dt$$

$$SG_{Ang}(Deg.\sec) = \int_0^T |\Delta \delta_{SG}| dt \tag{6}$$

$$SG_{Spd}(PU.\sec) = \int_0^T |\Delta \omega_{SG}| dt$$

$$SG_{Power}(PU.\sec) = \int_0^T |\Delta P_{SG}| dt$$

$$PV_{DCvlt}(PU.\sec) = \int_0^T |\Delta V_{PVDCvlt}| dt$$

where ΔP_{DFIG}, $\Delta \omega_{DFIG}$, ΔV_{DFIGdc}, $\Delta \delta_{SG}$, $\Delta \omega_{SG}$, ΔP_{SG}, $\Delta P_{PVDCvlt}$ represent power deviation of DFIG, speed deviation of DFIG, DC link voltage deviation of DFIG, load angle deviation of SG, rotor speed deviation of SG, power deviation of SG, and DC-link voltage deviation of PV, respectively. Lower values of the indices indicate improved system performance.

4. Simulation results and discussion

This segment presents simulation outcomes that validate the enhancement in transient stability of the suggested hybrid power system by implementing four CPD-FCL techniques. MATLAB/SIMULINK software was utilized to conduct simulations, encompassing both balanced (three-phase to ground (3lg)) and unbalanced (line to ground (1lg)) faults occurring at point A, as depicted in Fig. 1.Variation of power generation in hybrid power systems is modelled by employing two different power generation capacities (100% and 40%). The occurrence of faults is assumed to happen at 0.1 seconds, and the breakers connected to the faulty line are opened at 0.2 seconds (after 6 cycles) and reclosed at 1.1 seconds (after 60 cycles). Additionally, the simulation encompasses a total time span of 3.0 seconds, with a time step of 0.00001 seconds. To analyze the transient stability of the hybrid power system, the potential impacts of both balanced and unbalanced faults, as well as power generation capacity, are taken into account. This is achieved by considering three distinct scenarios.

Table 2. Scenarios considering different fault and generation conditions.

Scenario	Fault	Power generation capacity (%)
Scenario I	balanced 3lg	100
Scenario II	unbalanced 1lg	100
Scenario III	balanced 3lg	40

Stability performance of the grid in response to using CPD-FCL configurations (DVR-BFCL, DVR-SFCL, UPQC-BFCL and UPQC-SFCL) within all three scenarios are investigated. Furthermore, for the sake of comparison, transient response of the power system under the same faults but with using BFCL, SFCL and without FCL are analyzed. Table 3 presents fault limiting methods used in this study including energy storing and losing features of each method.

Table 3. Energy compensating and losing features of fault limiting methods applied in this study.

Technique	Without FCL	BFCL	SFCL	DVR-BFCL	DVR-SFCL	UPQC-BFCL	UPQC-SFCL
Energy compensating				✓	✓	✓	✓
Energy losing		✓	✓	✓	✓	✓	✓

4.1 Scenario I

This scenario considers the hybrid power system shown in Fig. 1with full power generation capacity under balanced 3lg fault. Transient stability of the system is investigated based on performance indices of SG, PV and DFIG formulated in Eq 6.Figs 12, 13, and 14 illustrate transient performance of PV DC link, SG and DFIG under 3lg fault while the power generation capacity is at the maximum level. As shown in Fig. 12, utilizing CPD-FCL technology configuration (DVR-BFCL, DVR-SFCL, UPQC-BFCL and UPQC-SFCL) resulted in lower rates of PV DC-link voltage (PV_{DCvlt}) proving the transient stability improvement. Table 4 presents obtained values of transient performance indices for PV DC link under balanced 3lg fault. The transient response of SG is presented via simulation results of the SG load angle, real power, rotor speed, and terminal voltage in Fig. 13(a)-(d), respectively. According to Eq 6, these are SG transient performance indices, and obtained values reported in Table 4indicate improved transient stability. Rotor speed, terminal voltage, real power, and DC link of DFIG shown in Fig. 14 (a)-(d) presents transient stability of DFIG system in response to using FCLs assumed in this experiment. Table 4 also reports values obtained for performance indices of DC link of DFIG.
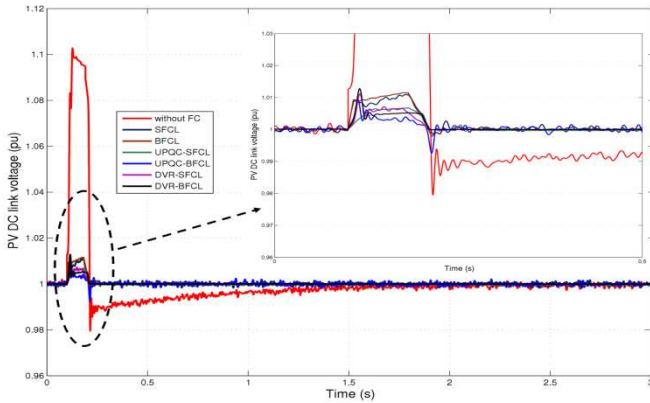
Fig. 12. Comparative transient responses of PV DC link subject to 3lgfault and full energy generation capacity.

Table 4. Values of performance indices obtained in scenario I.

3lg	Without FCL	BFCL	SFCL	DVR-BFCL	DVR-SFCL	UPQC-BFCL	UPQC-SFCL
SG_{ang}(deg.sec)	28.14	9.77	11.3	7.5	6.6	6	8
SG_{spd}(pu.sec)	0.037	0.019	0.021	0.0162	0.0153	0.014	0.0165
SG_{pow}(pu.sec)	1.39	0.192	0.315	0.094	0.088	0.079	0.106
SG_{vlt}(pu.sec)	0.21	0.103	0.12	0.06	0.05	0.040	0.062
$DFIG_{spd}$(pu.sec)	0.132	0.105	0.113	0.84	0.085	0.078	0.091
$DFIG_{vlt}$(pu.sec)	0.71	0.320	0.375	0.224	0.218	0.213	0.232
$DFIG_{pow}$(pu.sec)	0.172	0.061	0.073	0.052	0.054	0.048	0.057
PV_{dcvlt}(pu.sec)	2.502	1. 59	1.68	1.142	1.105	1.088	1.169

4.2 Scenario II

Second scenario contains transient performance analysis of the projected hybrid power system operating with full generation capacity under unbalanced 1lg fault. Like the first scenario, transient responses of PV DC link, SG and DC link of DFIG to proposed fault control techniques have been simulated. Simulation results were validated by evaluating performance indices formulated in Eq 6.

Fig. 15 depicts transient response of SG under conditions assumed within the scenario II. Simulation results obtained for SG system were validated using SG load angle (Fig. 15 (a)), SG real power (Fig. 15 (b)), SG rotor speed (Fig. 15 (c)), and SG terminal voltage (Fig. 15 (d)). Accurate values of these performance indices have been presented in Table 5 comparing these values proves the considerable influence of using energy compensating devices (DVR and UPQC) with conventional energy-losing FCL technologies (BFCL and SFCL) on limiting the fault currents and improving transient stability in the power system under study.
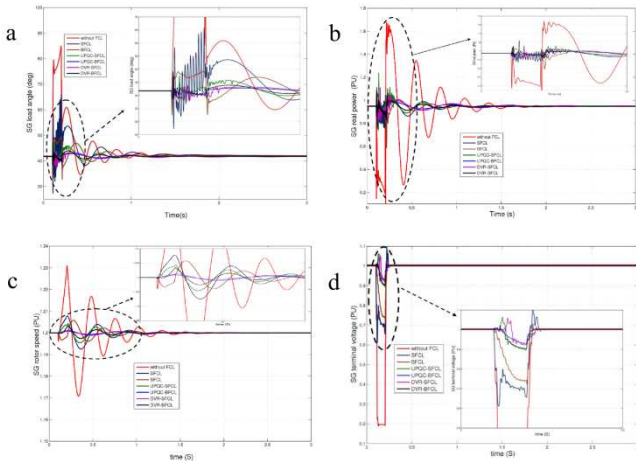
Fig. 13. Comparative transient responses of SG subject to 3lg fault and full energy generation capacity: (a) SG load angle, (b) SG real power, (c) SG rotor speed and (d) SG terminal voltage.
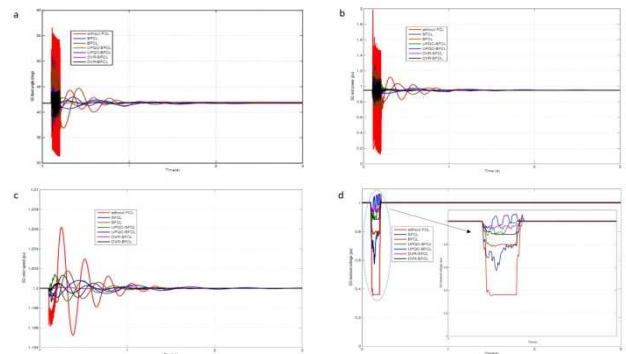
Fig. 15. Comparative transient responses of SG subject to 1lg fault and full energy generation capacity of DGs: (a) SG load angle, (b) SG real power, (c) SG rotor speed and (d) SG terminal voltage.

The transient performance of DC link DFIG in response to applying planned control techniques under the conditions assumed within scenario II have been evaluated through DFIG terminal voltage ($DFIG_{Vterminal}$) index.
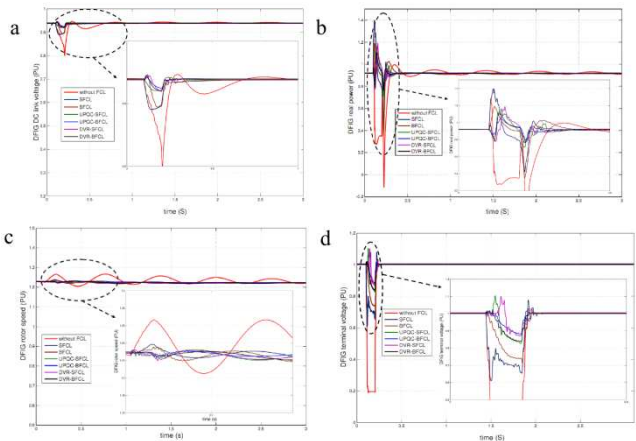
Fig. 14. Comparative transient responses of DC link DFIG subject to 3lg fault and full energy generation capacity of DGs: (a) DFIG DC link voltage, (b) DFIG real power, (c) DFIG rotor speed, (d) DFIG terminal voltage.

Fig. 16 depicts simulation results of DFIG terminal voltage, where UPQC-BFCL energy compensating technique shows the maximum stability improvement. Detailed information about obtained values of DFIG performance indices are available in Table 5.
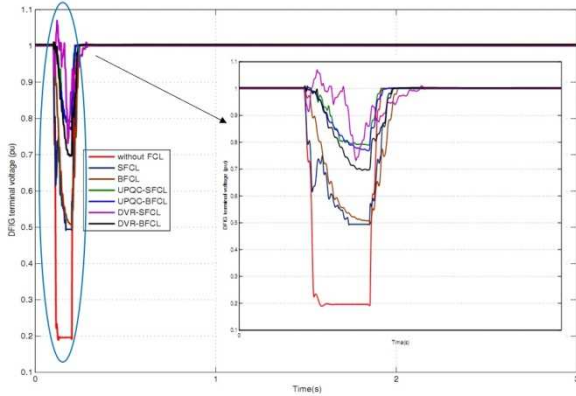
Fig. 16.DFIG terminal voltage under 1lg fault and considering full energy generation capacity of the system under study.

Table 5. Values of performance indices obtained in scenario II.

1lg	Without FCL	BFCL	SFCL	DVR-BFCL	DVR-SFCL	UPQC-BFCL	UPQC-SFCL
SG_{ang}(deg.sec)	18.7	4.3	5.1	2.8	2.4	**2.1**	3.4
SG_{spd}(pu.sec)	0.014	0.0086	0.0072	0.0048	**0.0045**	0.0056	0.0077
SG_{pow}(pu.sec)	0.64	0.082	0.05	0.037	**0.028**	0.052	0.057
SG_{vlt}(pu.sec)	0.15	0.107	0.13	0.072	0.054	**0.045**	0.066
$DFIG_{spd}$(pu.sec)	0.102	0.082	0.94	0.074	0.063	**0.055**	0.081
$DFIG_{vlt}$(pu.sec)	0.62	0.382	0.45	0.285	0.23	**0.221**	0.311
$DFIG_{pow}$(pu.sec)	0.13	0.052	0.068	0.056	**0.044**	0.055	0.052
PV_{dcvlt}(pu.sec)	1.3	0.705	0.65	0.42	0.46	**0.38**	0.41

4.3 Scenario III

This scenario reflects the importance of variation of energy generation capacity on limiting fault current and consequently improving transient stability in power system. Comparing with previous scenarios, maximum energy generation capacity of involved DG sources has been reduced from 100% (Scenarios I and II) to 40% in this scenario. Balanced 3lg type of fault was assumed in scenario III.

Fig. 17 demonstrates impressive transient stability improvement of SG validated by four performance indices: SG load angle (Fig. 17 (a)), SG real power (Fig. 17 (b)), SG rotor speed (Fig. 17 (c)), and SG terminal voltage (Fig. 17 (d)). The comparison among applied options shows that UPQC-BFCL and DVR-SFCL are the best solutions to boost transient stability of the proposed system in this scenario. Table 6gives the rates obtained for each SG performance indices. Furthermore, DFIG terminal voltage subject to 3lg fault and 40% energy generation capacity of DGs has been depicted in Fig. 18.
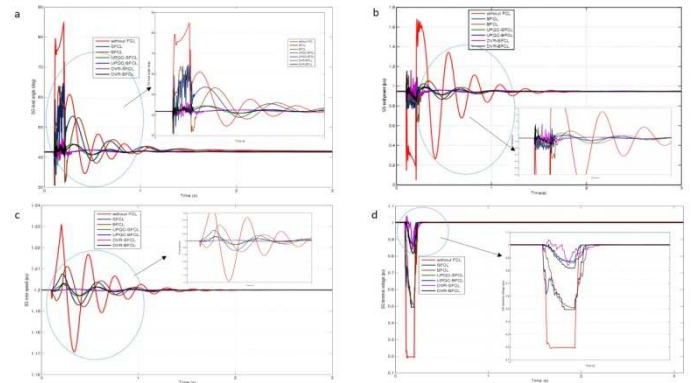
Fig. 17. Comparative transient responses of SG subject to 3lg fault and 40% energy generation capacity: (a) SG load angle, (b) SG real power, (c) SG rotor speed and (d) SG terminal voltage.
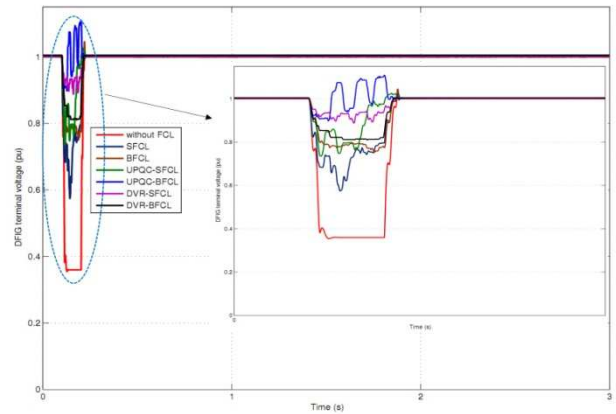
Fig. 18.DFIG terminal voltage subject to 3lg fault and 40% energy generation capacity of DGs.

Table 6. Values of performance indices obtained in scenario III, during 3lg fault and 40% Capacity of DGs.

3lg	Without FCL	BFCL	SFCL	DVR-BFCL	DVR-SFCL	UPQC-BFCL	UPQC-SFCL
Sg_{ang}(deg.sec)	28.14	14.3	11.5	8.2	7.1	**6.6**	9
Sg_{spd}(pu.sec)	0.037	0.019	0.021	0.0138	**0.01**	0.011	0.0152
Sg_{pow}(pu.sec)	1.39	0.196	0.292	0.082	0.052	**0.049**	0.94
Sg_{vlt}(pu.sec)	0.21	0.103	0.128	0.064	0.058	**0.046**	0.062
$dfig_{spd}$(pu.sec)	0.132	0.107	0.123	0.89	0.086	**0.08**	0.101
$dfig_{vlt}$(pu.sec)	0.71	0.48	0.52	0.29	**0.22**	0.27	0.25
$dfig_{pow}$(pu.sec)	0.62	0.024	0.02	0.018	**0.014**	0.017	0.015
PV_{dcvlt}(pu.sec)	2.502	1. 69	1.88	1.184	**1.115**	1.128	1.179

4.4 Comparison of scenarios I, II, and III

Comparing the results indicates that UPQC-BFCL demonstrates superior transient performance for the PV DC link in scenarios I and II. On the other hand, DVR-SFCL achieves the best performance in scenario III. It is important to highlight that when a fault occurs, there is a sudden decrease in voltage at the PCC, leading to reduced power fed into the grid. However, the DC/DC converter can

supply the maximum available PV power to the DC link. As a consequence of the power imbalance between the PCC and the injected power, the DC link voltage experiences a sharp increase, as depicted in Fig. 12.

Figs. 13 and 14 illustrate transient responses of rotating-type DG sources in scenario I that have approximately similar performances. Without applying control schemes, the current rises abruptly in the fault situation and terminal voltage of both SG (Fig. 13 (d)) and DFIG (Fig. 14 (d)) drop down to 20%. Furthermore, when a fault occurs, the actual power injected into the grid by the Synchronous Generator (SG) and Doubly Fed Induction Generator (DFIG) significantly decreases, as depicted in Fig. 13 (b) and Fig. 14 (b), respectively. Consequently, the mechanical power of both the SG and DFIG cannot be converted into electrical power, leading to excessive stress on the mechanical components of these rotating machines and an increase in the rotational speed of their rotors, as demonstrated in Fig. 13 (c) and Fig. 14 (c) respectively. As a result, the electromagnetic torque of both the SG and DFIG experiences a sudden reduction since it is directly proportional to the square of the terminal voltage.

Considering the simulation results shown in Figs. 15 and 16 as well as values of performance indices of involved DG sources in Table 15, it is clear that UPQC-BFCL and DVR-SFCL are two best solutions to limit 1lg fault and improve the transient performance of DGs in scenario II. In scenario III, by reducing the energy generation capacity of DGs to 40% and assuming 3lg fault, obtained results shown in Figs. 17 and18 and Table 6 prove the efficiency of UPQC-BFCL and DVR-SFCL methods in increasing transient stability of the proposed hybrid system.

Comparison of results obtained in scenarios I and III show that suggested storing-losing configurations (DVR-BFCL, DVR-SFCL, UPQC-BFCL, and UPQC-SFCL) have less sensitivity (index deviation) to DGs generation capacity and more stability than conventional FCLs (BFCL,SFCL). Also, the comparison between transient performance of rotating DGs (DFIG and SG) and fixed DG (PV) in all three scenarios reveal that storing-losing techniques have superior performance than using single FCLs. The utilization of FCL significantly improves the system performance, as evidenced by the simulation results and performance indices. Without incorporating FCL, the system demonstrates the poorest performance.

5. Conclusion

Configurations of CPDs and FCLs relying on energy compensating feature of CPDs improved the transient performance of DG sources. The validation of the proposed approach involved assessing its efficacy across three distinct scenarios, encompassing both balanced and unbalanced fault types. Also, consequence of variable energy generation capacity of involved DGs has been taken into account in these scenarios. Simulation results in scenarios I and II confirm the effective contribution of applied techniques to stabling the hybrid power system operating in 100% DG generation capacity regardless of types of faults (balanced and unbalanced). However, UPQC-BFCL has the best transient performance in three phase-ground (3lg) balanced fault.

The comparison among all three scenarios (considering balanced and unbalanced faults and DG generate fluctuation) confirms that energy compensating-losing method (DVR-BFCL, DVR-SFCL, UPQC-BFCL, and UPQC-SFCL) have better performance than BFCL and SFCL. When comparing scenarios I and III with similar faults but different shares of DG energy generation (100% and 40%), it is notable that transient performance of all FCLs decreases with allocating lower DG generation capacity (40%). Even, performance reduction is bigger for conventional BFCL and SFCL.

Appendix

Table 7. DFIG parameters.

Parameter	Value
Nominal power	150 *kW*
Rated voltage	575 *V*
Stator to rotor turns ratio	0.3
Rated frequency	60 *Hz*
Stator resistance (Rs)	0.013 *p.u.*
Stator inductance (Ls)	0.000284 *H*
Rotor resistance (Rr)	0.005 *p.u.*
Rotor reactance (Lr)	0.00282 *H*
Mutual inductance (Lm)	0.01425 *H*
Inertia constant (H)	0.6 *Kg.m²*
DC link rated voltage	1150 *V*
Turbine inertia constant	4.32 *Kg.m²*
Shaft spring constant	1.5 *p.u.*
Shaft mutual damping	1.11 *p.u.*

Table 8. SG parameters.

Parameter	Value
Nominal power	111 *kW*
Rated voltage	575 *V*
Rated frequency	60 *Hz*
Stator resistance (Rs)	0.56 Ω
Stator inductance (Ls)	0.00714 *H*
d-axis inductance (Lmd)	0.005 *p.u.*
q-axis inductance (Lmq)	0.00282 *H*
Inertia constant (H)	2.4 *Kg.m²*
Pole pairs	2

Table 9. BFCL parameters.

Parameter	Value
Transition response time	100 *ms*
Shunt resistance	0.829 *p.u.*
L_{DC}	0.01 *H*
R_{DC}	0.001 Ω

Table 10. SFCL parameters.

Parameter	Value
Transition response time	2 *ms*
Minimum impedance	0.01 Ω
Maximum impedance	4 Ω
Triggering current	200 *A*
Recovery time	10 *ms*

Table 11. DVR parameters.

Parameter	Value
DC link capacitor	1500 *uF*
DC link nominal voltage	1200 *V*
Series filter inductor	70.36 *mH*
Series filter capacitor	100 *uF*

Table 12. UPQC parameters.

Parameter	Value
DC link capacitor	1500 *uF*
DC link nominal voltage	1200 *V*
Series filter inductor	70.36 *mH*
Series filter capacitor	100 *uF*
Parallel filter inductor	70.36 *mH*
Parallel filter capacitor	100 *uF*

References

[1] V. Telukunta, J. Pradhan, A. Agrawal, M. Singh, and S. G. Srivani, "Protection challenges under bulk penetration of renewable energy resources in power systems: A review," *CSEE Journal of Power and Energy Systems*, vol. 3, no. 4, pp. 365–379, 2017, doi: 10.17775/cseejpes.2017.00030.

[2] X. Liang, "Emerging Power Quality Challenges Due to Integration of Renewable Energy Sources," *IEEE Transactions on Industry Applications*, vol. 53, no. 2, pp. 855–866, 2017, doi: 10.1109/TIA.2016.2626253.

[3] M. S. Alam, M. A. Y. Abido, and I. El-Amin, "Fault current limiters in power systems: A comprehensive review," *Energies*, vol. 11, no. 5, 2018, doi: 10.3390/en11051025.

[4] T. M. Masaud and R. D. Mistry, "Fault current contribution of Renewable Distributed Generation: An overview and key issues," *2016 IEEE Conference on Technologies for Sustainability, SusTech 2016*, pp. 229–234, 2017, doi: 10.1109/SusTech.2016.7897172.

[5] S. Xia, Q. Zhang, S. T. Hussain, B. Hong, and W. Zou, "Impacts of integration of wind farms on power system transient stability," *Applied Sciences (Switzerland)*, vol. 8, no. 8, 2018, doi: 10.3390/app8081289.

[6] M. K. Hossain and M. H. Ali, "Transient Stability Augmentation of PV/DFIG/SG-Based Hybrid Power System by Nonlinear Control-Based Variable Resistive FCL," *IEEE Transactions on Sustainable Energy*, vol. 6, no. 4, pp. 1638–1649, 2015, doi: 10.1109/TSTE.2015.2463286.

[7] S. Yadav, G. K. Choudhary, and R. K. Mandal, "Review on Fault Current Limiters," *International Journal of Engineering Research & Technology (IJERT)*, vol. 3, no. 4, pp. 1595–1604, 2014.

[8] R. Rajan and F. M. Fernandez, "Power control strategy of photovoltaic plants for frequency regulation in a hybrid power system," *International Journal of Electrical Power and Energy Systems*, vol. 110, no. January, pp. 171–183, 2019, doi: 10.1016/j.ijepes.2019.03.009.

[9] M. Zolfaghari, R. M. Chabanlo, M. Abedi, and M. Shahidehpour, "A Robust Distance Protection Approach for Bulk AC Power System Considering the Effects of HVDC Interfaced Offshore Wind Units," *IEEE Systems Journal*, vol. 12, no. 4, pp. 3786–3795, 2018, doi: 10.1109/JSYST.2017.2760139.

[10] R. B. Leslie Hewitson, Mark Brown, *Practical Power System Protection*, 1st Editio. 2004.

[11] A. Abramovitz and K. Ma Smedley, "Survey of solid-state fault current limiters," *IEEE Transactions on Power Electronics*, vol. 27, no. 6, pp. 2770–2782, 2012, doi: 10.1109/TPEL.2011.2174804.

[12] P. N. Vovos, H. Song, K. W. Cho, and T. S. Kim, "A network reconfiguration algorithm for the reduction of expected fault currents," *IEEE Power and Energy Society General Meeting*, 2013, doi: 10.1109/PESMG.2013.6673000.

[13] P. N. Vovos and J. W. Bialek, "Impact of fault level constraints on the economic operation of power systems," *2005 IEEE Russia Power Tech, PowerTech*, vol. 21, no. 4, pp. 1600–1607, 2005, doi: 10.1109/PTC.2005.4524420.

[14] A. Safaei, M. Zolfaghari, M. Gilvanejad, and G. B. Gharehpetian, "A survey on fault current limiters: Development and technical aspects," *International*

Journal of Electrical Power and Energy Systems, vol. 118, no. December 2019, p. 105729, 2020, doi: 10.1016/j.ijepes.2019.105729.

[15] L. Chen *et al.*, "Application of a modified flux-coupling type superconducting fault current limiter to transient performance enhancement of micro-grid," *Physica C: Superconductivity and its Applications*, vol. 518, pp. 144–148, 2015, doi: 10.1016/j.physc.2015.02.051.

[16] D. H. Choi, J. I. Yoo, D. Kim, S. H. Lee, and J. W. Park, "Analysis on Effect of SFCL Applied to an Isolated Microgrid with a Dynamic Load Model," *IEEE Transactions on Applied Superconductivity*, vol. 27, no. 4, pp. 13–16, 2017, doi: 10.1109/TASC.2017.2652488.

[17] L. Chen *et al.*, "Application and Design of a Resistive-Type Superconducting Fault Current Limiter for Efficient Protection of a DC Microgrid," vol. 29, no. 2, 2019.

[18] D. M. Yehia, D. A. Mansour, and S. Member, "Modeling and Analysis of Superconducting Fault Current Limiter for System Integration of Battery Banks," vol. 28, no. 4, pp. 13–18, 2018.

[19] S. A. A. Shahriari *et al.*, "Minimizing the Impact of Distributed Generation on Distribution Protection System by Solid State Fault Current Limiter," pp. 7–13, 2010.

[20] M. M. R. Ahmed, G. A. Putrus, L. Ran, and L. Xiao, "Harmonic Analysis and Improvement of a New Solid-State Fault Current Limiter," vol. 40, no. 4, pp. 1012–1019, 2004.

[21] G. Chen, D. Jiang, Z. Lu, Z. Wu, and A. Topology, "A New Proposal for Solid State Fault Current Limiter and Its Control Strategies."

[22] J. P. Sharma and H. R. Kamath, "Influence of Solid State Fault Current Limiter on Grid Connected Photovoltaic System Protection," *Journal of Clean Energy Technologies*, vol. 6, no. 3, pp. 254–257, 2018, doi: 10.18178/jocet.2018.6.3.470.

[23] W. P. Generation, A. R. Fereidouni, B. Vahidi, S. Member, and T. H. Mehr, "The Impact of Solid State Fault Current Limiter on Power Network With," vol. 4, no. 2, pp. 1188–1196, 2013.

[24] A. M. Hamada, S. S. M. Ghoneim, S. A. Mohamed, S. Walid, and E. Abdellatif, "International Journal of Electrical Power and Energy Systems Performance analysis of three-phase hybrid fault current limiter with one commutation circuit," *International Journal of Electrical Power and Energy Systems*, vol. 133, no. June, p. 107297, 2021, doi: 10.1016/j.ijepes.2021.107297.

[25] M. Ebrahimpour, B. Vahidi, S. Member, and S. H. Hosseinian, "A Hybrid Superconducting Fault Current Controller for DG Networks and Microgrids," vol. 23, no. 5, 2013.

[26] P. M. Tripathi and K. Chatterjee, "International Journal of Electrical Power and Energy Systems Real-time implementation of ring based saturated

core fault current limiter to improve fault ride through capability of DFIG system," *International Journal of Electrical Power and Energy Systems*, vol. 131, no. March, p. 107040, 2021, doi: 10.1016/j.ijepes.2021.107040.

[27] Y. Pal, A. Swarup, S. Member, B. Singh, and S. Member, "A Review of Compensating Type Custom Power Devices for Power Quality Improvement."

[28] S. Singh, "Various Custom Power Devices for Power Quality Improvement : A Review," pp. 689–695, 2018.

[29] "29. View of Recent Trends in Power Quality Improvement Using Custom Power Devices and Its Performance Analysis.pdf." .

[30] N. S. Chouhan, "Doubly fed induction generator with integrated energy storage system for smoothening of output power," pp. 1–108, 2010.

[31] G. Rashid, S. Member, M. H. Ali, and S. Member, "Transient Stability Enhancement of Doubly Fed Induction Machine-Based Wind Generator by Bridge-Type Fault Current Limiter," vol. 30, no. 3, pp. 939–947, 2015.

[32] K. Hossain and M. H. Ali, "Transient stability augmentation of PV / DFIG / SG-based hybrid power system by parallel-resonance bridge fault current limiter," vol. 130, pp. 89–102, 2016.

[33] G. Didier and J. Lévêque, "Electrical Power and Energy Systems Influence of fault type on the optimal location of superconducting fault current limiter in electrical power grid," *International Journal of Electrical Power and Energy Systems*, vol. 56, pp. 279–285, 2014, doi: 10.1016/j.ijepes.2013.11.018.

[34] A. Moghadasi, A. Sarwat, and J. M. Guerrero, "A comprehensive review of low-voltage-ride-through methods for fi xed-speed wind power generators," *Renewable and Sustainable Energy Reviews*, vol. 55, pp. 823–839, 2016, doi: 10.1016/j.rser.2015.11.020.

[35] A. J. Laxmi, K. U. Rao, M. Sushama, and N. T. Devi, "Hardware Implementation Of Single Phase Dynamic Voltage Restorer," pp. 204–209, 2010.

[36] A. A. Hussein and M. H. Ali, "Comparison among series compensators for fault ride through capability enhancement of wind generator systems," *International Journal of Renewable Energy Research*, vol. 4, no. 3, pp. 767–776, 2014.